2024 IEEE/RSJ International Conference on Intelligent Robots and Systems (IROS)
October 14-18, 2024. Abu Dhabi, UAE

Portable robot for needle insertion assistance to femoral artery

Zhuoqi Cheng[1,*], Bence Mány[2], Kasper Balsby Jørgensen[1], Siheon An[3], Marcus Leander Jensen[2], Richard Thulstrup[2], Habib Frost[2], Thiusius R. Savarimuthu[1], and Olof Huldt[2]

***Abstract*— Femoral artery access is a common and critical procedure for various cardiovascular interventions. Although it is a time critical operation, accessing the Common Femoral Artery (CFA) typically requires expertise found in specialized medical settings. The necessity for specialized personnel or transport to equipped facilities can lead to delays, potentially exacerbating patient outcomes. To address this challenge, a portable and cost-effective robotic device that autonomously localizes a CFA and precisely positions a needle guide is developed. Through the needle guide, needle can be quickly and accurately inserted into the artery even by non-specialist physicians. Different from the conventional B-mode ultrasound guided procedure, the proposed robotic solution utilizes a Doppler transducer for detecting the arterial location and employs a single M-mode transducer for depth measurement. A series of experiments are designed and conducted to validate the system's feasibility, achieving high accuracy within 2 mm, rapid processing within 1.5 min, and a 100% success rate, thus proving the system's efficacy. These results convince us for further refinement of the system and support its evaluation in animal studies.**

***Index Terms*— Needle insertion robot, Robot assisted sensing, femoral artery access, ultrasound robot, signal processing.**

I. Introduction

Femoral artery access is essential for a wide range of cardiovascular procedures such as diagnostic angiography, percutaneous coronary intervention (PCI), and structural heart interventions. This site is pivotal for deploying hemodynamic support devices like intraaortic balloon pumps and extracorporeal membrane oxygenation (ECMO), and is often chosen for arterial access in invasive monitoring, despite the growing preference for radial access. The expertise required for femoral artery access, typically available in specialized settings, and the possible delays in accessing such care highlight the need for readily accessible emergency solutions. Techniques like REBOA (Resuscitative Endovascular Balloon Occlusion of the Aorta) for controlling bleeding further emphasize the urgency of improving access to femoral artery interventions, potentially saving an estimated 10,000 lives annually [1].

Ultrasound (US) guided needle insertion to CFA is a widely used technique. Practitioners utilize US imaging to locate the CFA and track the needle tip position during insertion. Compared to blind insertion, US-guided approach is generally associated with higher success rate and less insertion time [2]. While US-guided CFA insertion improves safety and efficiency, there are still some remaining challenges. Firstly, US-guided procedures necessitate specialized training to attain proficiency. Such proficiency include not just in operating the US device but also in interpreting real-time images for accurate needle placement. Secondly, real-time US guidance requires significant hand-eye coordination and dexterity to simultaneously manipulate the probe and perform the insertion [3]. These skills can only be developed over time with practice. Also, the availability of US equipment can be another limiting factor due to their size and cost. This becomes particularly problematic in low-resource settings or emergency scenarios outside hospitals, where such equipment may not be readily available.

Previous studies has highlighted the significant potential of robotic technologies to enhance the precision and efficacy of needle-based interventions [4], [5]. Zevallos *et al.* presented a teleoperated robot, integrating B-mode US and needle insertion in a single robotic arm to streamline femoral vascular access [6]. Additionally, Koskinopoulou *et al.* introduced a dual robot system, with one robot managing the US probe for artery detection and another executing needle insertion [7]. Nevertheless, most existing technologies do not meet the criteria for portability. According to the authors' knowledge, the design by Brattain *et al.* may be the only handheld robotic device specifically for femoral artery access in needle-based procedures, which incorporates an artificial intelligence (AI) based US image processing [8].

The above innovations represent significant strides in robotic-assisted CFA intervention procedure. To the best of the authors' knowledge, the technology introduced herein represents the world's first portable and cost-effective robot designed for autonomously guiding needle-based procedures to access the CFA. To ensure portability, we developed a unique robot-assisted sensing system that utilizes a Doppler sensor for lateral localization of the CFA and an M-mode US sensor to measure its depth. Upon locating the CFA, the robot accurately positions a needle guide. This guide enables healthcare practitioners to insert a needle into the artery, thereby improving the success rate and efficiency of CFA access procedures.

After the Introduction section, more medical and technical backgrounds are presented in Section II. In Section III and Section IV, we describe the design of the robotic system and signal processing algorithms respectively. The system characterization and experiments are described in Section

Z. Cheng, K. B. Jørgensen and T. R. Savarimuthu were with MMMI, SDU, Odense, 5230 Denmark.

B. Mány, M. L. Jensen, R. Thulstrup, H. Frost, and O. Huldt were with Neurescue ApS.

S. An was with School of Mechanical Engineering, Chonnam National University, Gwangju, 61186, South Korea.

Corresponding author: Z. Cheng. (zch@mmmi.sdu.dk)

This study is supported by the Innovation Fund Denmark under the agreement 1061-00071A.

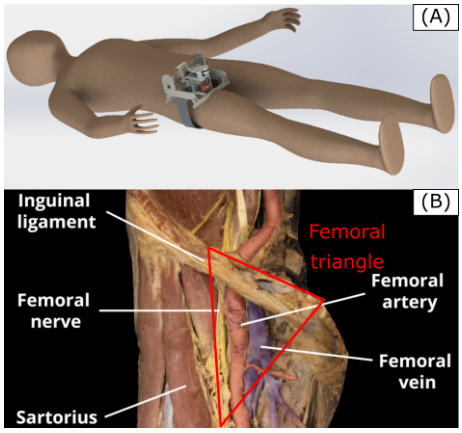

Fig. 1. (A) The portable robot is secured to the thigh of the patient using a belt for use. (B) The CFA is located in the groin area, which can be accessed through needle insertion slightly below the inguinal ligament.

V. We provide the experimental results in Section VI and discussion in Section VII. Section VIII concludes this study.

II. Background

A. CFA anatomy

The designed robot aims to assist needle insertion to a CFA through the femoral triangle in the thigh as shown in Fig. 1. The femoral artery lies deep within soft tissues, making its direct visualization nearly impossible. The femoral artery average outer diameter ranges from 6 to 10 mm for normal adult [9], and its typical depth beneath the skin surface ranges from 1 to 2 cm. The flow rate of blood through the femoral artery is relatively high, approximately 70-80 mL/s, and it circulates under substantial pressure typically ranging from 90/60 mmHg to 120/80 mmHg. The artery is typically identified by its pulsatile flow through palpation. In invasive procedures involving an incision, the CFA distinguished by its distinct red color, indicating oxygen-rich blood.

B. Ultrasound techniques in medical application

The above anatomical analysis, particularly the distinction between blood and surrounding soft tissues, as well as the pulsatile characteristics of CFA, indicates the efficacy of US sensing for determining the artery's location.

The principle of US technology involves the transducer emitting and receiving US waves by converting electrical energy into mechanical vibrations and back. When the US waves encounter boundaries between different tissues or structures, such as the interface between soft tissue and blood, a portion of the waves reflects back to the transducer. These reflected sound waves are captured by the US device, which then translates them into electrical analog signals.

The US techniques can be classified to the following:

- **A-mode:** one-dimensional spikes representing the depth of the reflecting surfaces, which uses a single element transducer.
- **B-mode:** the standard US imaging method for diagnostics, creates two-dimensional cross-sectional images, using an array of transducers.
- **M-mode:** tissue motion capture by sampling a single line through the tissue over time, and creating the image by appending consecutive A-mode signals.
- **Doppler:** the measure of the velocity of moving objects, such as blood flow, by analyzing the change in frequency of the US wave due to the Doppler effect.

C. Portable robotic solution

In this study, we choose to use two kinds of US techniques: M-mode and Doppler. While B-mode imaging is traditionally employed for identifying the CFA, it typically involves substantial equipment that is both costly and large. Also, distinguishing blood vessels in B-mode images requires complicated image processing techniques to differentiate them from background noise. Compared to B-mode imaging, M-mode and Doppler techniques utilize a single transducer, making them both cost-effective and compact, thereby aligning well with portability needs.

As shown in Fig. 1(A), the proposed device can be easily brought to the subject, and placed on the subject's thigh. The robot is required to perform the scanning to localize of the CFA. Subsequently, the needle guide's position is adjusted accordingly, so the medic can execute the needle insertion through the well-positioned needle guide. More technical details are provided in the following sections.

III. Robotic System Design

A. Mechanical design

Fig. 2(A) and (B) show the mechanical design of the portable robot in different views. To facilitate visibility, we change the transparency of the *Frame* and *Elastic belt*. The *Needle* shown in Fig. 2(A) and (B) is not a part of the robotic system. It will only be inserted manually after the robot locates the CFA and controls the *Needle guide* to the target position.

Actuator 1 is fixed on the *Frame*, and the connected *Lead screw 1* drives the *Carrier* to move horizontally. The *Mainbody* is connected to the *Carrier* through two pairs of rods, and constrained to slide vertically. In the *Mainbody*, we integrate a *M-mode transducer*, a *Doppler transducer*, a *Needle guide* and its driving system. The *M-mode transducer* is fixed on the *Mainbody* and oriented downward. The *Doppler transducer* is positioned at a 55° angle, and is able to adjust the depth via axial sliding. Additionally, the *Needle guide* is designed to move only in a vertical direction, with its motion controlled by *Actuator 2*. The position control is achieved through the coordination of *Lead screw 2* and a *timing belt*.

The robotic system's mechanical configuration allows for a horizontal scanning of 10 cm. The *Needle guide* is able to guide needle insertion at depths varying from 10 mm to 30 mm, covering most CFA anatomical depths. Additionally, springs are equipped between the *Carrier* and the *Mainbody*, as well as *Doppler transducer* and the *Mainbody*. As shown in Fig. 2(C) and (D), the springs provides a pre-load of about 10 N force for both the *M-mode transducer* and the *Doppler transducer*, assuring reliable body contact.

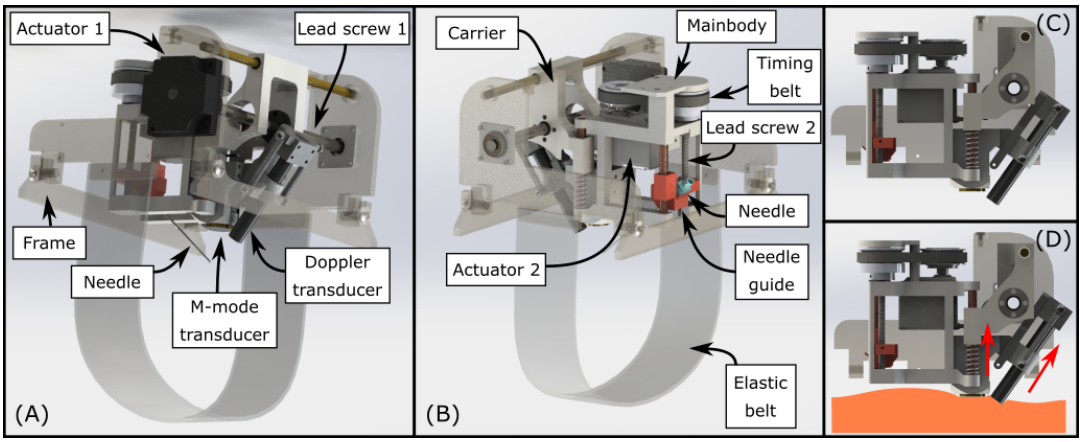

Fig. 2. (A)-(B) The mechanical model of the robot in different views. (C)-(D) Springs are used to provide about 10 N pre-load for both the *M-mode transducer* and the *Doppler transducer* when they are contacting the human body.

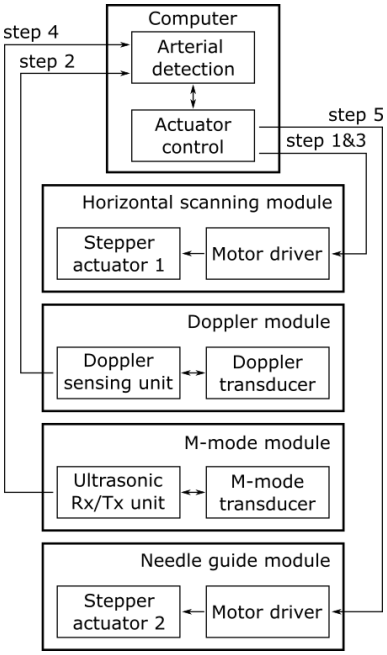

Fig. 3. The control schematics of the system.

B. Control system

The schematics of the robotic control system is shown in Fig. 3. The whole system comprises five main components: a computer, a horizontal scanning module, a Doppler module, a M-mode module and a needle guide module. The computer coordinates the operation of these modules, managing actuators, assimilating data, and processing signals for precise control and analysis. The horizontal scanning module employs a stepper motor (*Actuator 1*) coupled with a uStepper S32 driver, enabling precise positional adjustments under computer command. The Doppler module utilizes an UltraTec PD1v device, with a Teensy 3.6 microcontroller capturing audio signals for computer analysis at a rate of 200 Hz. The M-mode module features a 2.5P14 single-element transducer (Goworld Co., Ltd, China) and an ultrasonic device (US-Expert, Lecour electronique, France) transmitting data to the computer at 20 Hz. In addition, the needle guide module uses the same Teensy microcontroller to control a Parallax servo motor (*Actuator 2*), ensuring accurate needle positioning.

The operation starts with the initialization of all modules (Step 0). The *Needle guide* is lifted to its highest position, and the *Mainbody* is moved to the leftmost point. Both the M-mode module and the Doppler module are configured with the appropriate measurement parameters. Subsequently, a 10 cm horizontal scan is executed (Step 1) at a speed of 10 mm/s. During this procedure, the Doppler module continuously transmits signals to the computer at a 50 Hz sampling rate (Step 2). Upon completion of the scan, the computer analyzes the Doppler signals to determine the likely position of the CFA. Following this, *Actuator 1* relocates the *M-mode transducer* to above the identified CFA location (Step 3), and the M-mode module begins a continuous data logging session (Step 4). Based on received M-mode data, the computer calculates the depth of the CFA. Finally (Step 5), the *Needle guide* is adjusted to the estimated depth accordingly. Then it is ready for the practitioner to insert the needle.

IV. Algorithm for Arterial Detection & Localization

A. Doppler-based CFA localization

The complete Doppler signal, denoted as $s(t)$, is firstly subjected to detrending to remove an offset.

$$s_{det}(t) = s(t) - (m \cdot t + c) \tag{1}$$

where m and c represent the slope and intercept of the signal's linear trend, respectively. The resulting detrended signal, $s_{det}(t)$ is then processed through continuous wavelet transform (CWT), which decomposes the signal into a series of basis functions. Here, the Morlet wavelet function $\psi(t)$ is applied.

$$CWT(a,b) = \frac{1}{\sqrt{|a|}} \int_{-\infty}^{+\infty} s_{det}(t) \cdot \psi^* \left(\frac{t-b}{a} \right) dt \tag{2}$$

$$\psi(t) = \pi^{-1/4}\left(e^{i\omega_0 t} - e^{-\omega_0^2/2}\right)e^{-t^2/2} \tag{3}$$

where $\psi^*((t-b)/a)$ represents the complex conjugate of the wavelet function. Also, a is the scaling factor for adjusting the wavelet's stretch or compression, and b is the positional factor for shifting the wavelet along the time.

To extract the characteristics of the arterial signal, we compute the energy of CWT, denoted as E_D, by summing the squared absolute values of wavelet coefficients within a 2.6 s period and for a values ranging from 50 to 150. These parameter are chosen to encompass most spectrum information corresponding to the average adult human pulse.

$$E_D = \sum_{50}^{150}\sum_{t}^{t+2.6\,s} |CWT(a,b)| \tag{4}$$

Subsequently, the location of the CFA can be identified by applying a threshold to the calculated energy (E_D).

B. M-mode based CFA depth calculation

Upon receiving a set of A-mode signals, we firstly apply a band-pass filter along the depth axis for noise reduction, followed by an envelop operation. These techniques aim to enhance visualization of anatomical boundaries in the tissue, such as the walls of the CFA. After the above processing, we stack consecutive A-mode signals from the same position in order to create a M-mode 2-D representation, which is a dynamic view of the echo intensity in different depth over a temporal axis.

The generated M-mode signal is analyzed based on its temporal dynamics. Specifically, each segment of the signal at this fixed depth undergoes a Fast Fourier Transform (FFT) to translate the time-domain data into frequency domain. The signal's energy within a defined spectrum range (from 0.5 to 1.8 Hz) is calculated. This range is set given that the normal heart rate for a healthy adult at rest ranges between 60 to 100 beats per minute, and a slightly wider boundary can capture the arterial pulsation in most cases while filtering out noise. Then, the presence of the artery can be identified by finding the peak of the calculated energy within this spectrum range.

$$E_M = \sum_{f=0.5Hz}^{1.8Hz} |FFT(f)|^2 \tag{5}$$

Once the artery is identified, we calculate the distance based on the echo time using Equation (6). Here, Δs represents the distance from the transducer to the object, Δt denotes the time elapsed between the wave's transmission and its reception, and c is the velocity of wave propagation through the tissue. Considering that the wave travels to the artery and back, the full distance must be divided by 2.

$$\Delta s = \Delta t * c/2 \tag{6}$$

V. System Characterization and Experiments

This section presents the systematic characterization of the developed portable robot. Firstly, we focused on evaluating two key components: the M-mode transducer and Doppler transducer, both of which were based on a water tank setup. To accurately simulate physiological conditions, a pulsatile simulation pump was developed. Subsequently, the evaluation of the entire robotic system was undertaken, testing its integrated functionality and operational efficacy. The final phase of the experimentation involved the participation of human volunteer, providing a practical examination of the system's application in a clinical-like setting.

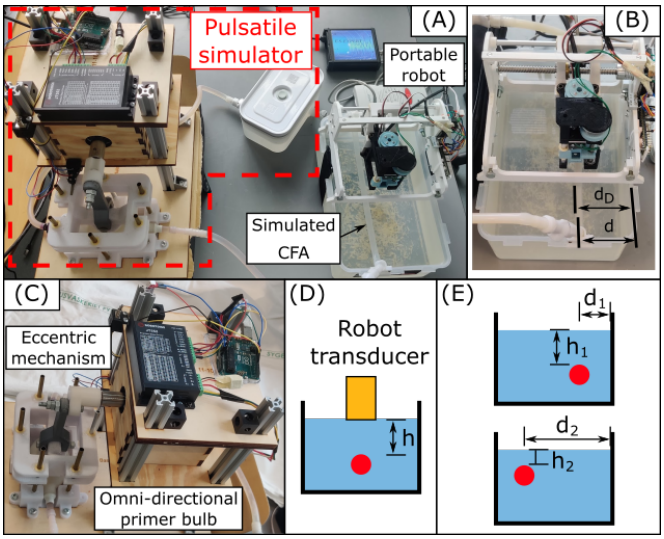

Fig. 4. (A) The experimental setup for characterizing the portable robot. (B) The right wall of the water tank is considered as the coordinate origin, and the detected tube position d_D is compared to the actual setting d. (C) A pulsatile pump is designed to simulate the arterial blood flow inside the tube. (D) Different depths h are set for the transducers' characterization. (E) In the whole system evaluation, the tube is placed in two places for a more comprehensive test.

A. Pulsatile simulation pump

A pulsatile simulation pump is designed to simulate the dynamics of systemic circulation in a patient. As shown in Fig. 4(C), the pump system operates by utilizing a stepper motor to propel a connected eccentric mechanism, which periodically exerts pressure on a primer bulb, mimicking the heart's systole and diastole. The cyclical pressure in the primer bulb generates a unidirectional flow, maintained by two check valves, one situated on the inlet side and the other on the outlet side, drawing parallels to the valves within the heart. Rice milk is used to simulate blood. It is pumped from a reservoir, inside plastic tubes, through a phantom, before returning to the same reservoir in a continuous loop, at a 1 Hz cycle. The flow rate of the pump is found approximately 500 ml/min, which is similar to the pulsatile nature of CFA 635 ml/min.Please refer to thesis [10] for more technical characteristics of the pulsatile pump.

B. Doppler transducer characterization

The experimental setup for Doppler transducer characaterization can be seen in Fig. 4. A water tank was used with a plastic tube secured between its side walls. The tube has an outer diameter of 10 mm and an inner diameter of 8 mm,

simulating an adult's CFA. The tube was connected to the pump, prescribed in Section V-A, to circulate pulsatile flow.

The robot was placed on the top of the water tank, where the tube was placed perpendicular to the robot's sliding axis. The *Elastic belt* on the robot passed through the bottom of the water tank to secure the robot's stability. The first step in the characterization study involved adjusting the tube's depth h, which was the top wall of the tube relative to the Doppler transducer's tip. Subsequently, the tank was filled with water until the tip of the transducer was submerged by a few millimeters. Next, the robot executed a 10 cm horizontal scan, during which Doppler signals were continuously recorded. Upon completion of the scan, the acquired signals were analyzed using the method detailed in section IV.A.

In this Doppler characterization study, we varied the depth h at increments of 10, 15, 20, and 25 mm, to span the typical depth range of the CFA, ensuring a comprehensive assessment across potential clinical scenarios.

C. M-mode transducer characterization

The setup for characterizing the M-mode transducer was similar to the Doppler study, which was also based on the water tank. In this procedure, we manually controlled *Actuator 1* to position the M-mode transducer directly above the tube. Then the depth between the tube's top wall and the tip of the M-mode transducer h was precisely adjusted. In this study, different settings of h including 10, 15, 20, and 25 mm were tested. Following this adjustment, the water tank was filled until the water's surface reached the tip of the transducer. Subsequently, the robot initiated the acquisition of A-mode samples by the transducer over a duration of 2 s. Upon completion of the signal acquisition, these samples were compiled for M-mode analysis.

D. System evaluation based on simulator

The full procedure of the robot in assisting needle insertion was assessed in this experiment, which was also carried out in the controlled water tank setup. To ensure robustness in our findings, the tube was placed in two different positions and depths for test. As shown in Fig. 4(E), the first configuration was established with a depth of h_1= 25 mm and a distance of d_1=30 mm. The second configuration was set at d_2=70 mm and h_2=10 mm. For each setting, the test was repeated three times. After the tube was placed to a predefined position and the water tank was filled, the robot commenced to perform the whole procedure automatically. This included conducting horizontal scans, employing Doppler analysis to localize the arterial analog, relocating the M-mode transducer precisely to above the identified location to measure and calculate the tube's depth, and then controlling the *Needle guide* to the determined depth. Subsequently, the experimenter would insert the needle through the guide with its whole length.

The primary metric for assessing the system's effectiveness was the success rate of inserting the needle into the tube.

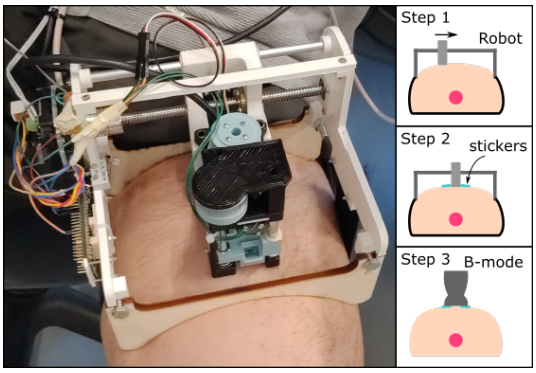

Fig. 5. The experimental setup for the preliminary system test with human subject.

In addition, we reported the completion time for the whole procedure as the indication of the the system's efficiency.

E. Preliminary system test on human volunteers

Furthermore, a simulated clinical environment was designed to evaluate the robotic system. One human volunteer participated in this study. Prior to the actual experiment, the volunteer was given information regarding the experimental objectives and procedure. Before and during the experiment, the subject was asked to remain relaxed and maintain a steady heart rate.

Fig. 5 illustrated the experimental procedure and the setup. The robot was placed on the subject's thigh near the groin area, with the *Needle guide* oriented towards the heart direction. Once the subject felt ready, the robot autonomously carried out the CFA localization and depth measurement procedure. It's important to note that no needle was inserted during these trials. Following the completion of the M-mode module's depth sensing, two small stickers were placed on the skin to mark the M-mode transducer's position. The robot was then carefully removed, and an experimenter manually positioned a B-mode US device (L15 wireless scanner, Clarius Ltd., UK) over the marked areas.

Through the B-mode imaging, we firstly confirmed whether the CFA presented. If so, its depth was measured and used as the benchmark for accuracy assessment.

VI. Results

A. Characterization results of Doppler and M-mode modules

Typical results of the Doppler module characterization during horizontal scanning in the water tank setup are presented in Fig. 6. The upper section shows the analog raw values over time and the lower section is its corresponding CWT. For each depth condition (h = 10, 15, 20, and 25 mm), the measurements were repeated five times. Then the presented arterial detection algorithm was applied to process the signal.

Two key metrics are considered for assessing the Doppler module, namely, the position error Δd and the tube diameter ϕ_D. By identifying the left and right boundaries of the detected positions, we calculate the tube's center d_D and compare this value with the ground truth value: $\Delta d = d - d_D$,

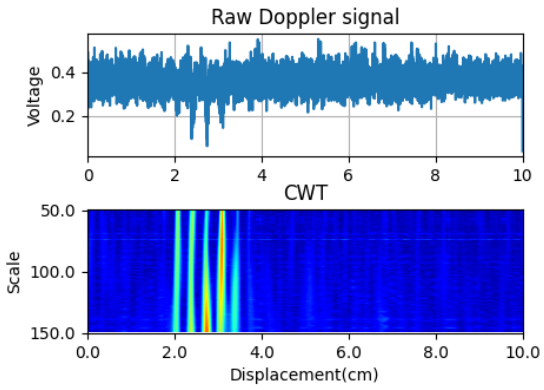

Fig. 6. An example of the raw Doppler signal and its corresponding CWT transform against the sensing displacement in water tank setup.

TABLE I

THE MEASURED HORIZONTAL ERROR Δd AND THE TUBE DIAMETER ϕ_D BASED ON THE DOPPLER SIGNAL.

h(mm)	15	20	25	30
Δd(mm)	0.9±0.3	0.7±0.4	0.7±0.1	1.1±0.5
ϕ_D(mm)	11.7±0.6	11.7±0.3	10.3±0.3	12.1±0.5

where the right wall of the water tank is the coordinate origin. In addition, the tube's diameter is estimated by measuring the difference between the last and first detected positions along the horizontal axis.

In all the trials, the embedded tube could always be detected by the robot. Table I summarizes the results of Δd and ϕ_D against different depth settings. The central errors for h_D of 10, 15, 20, and 25 mm are 0.9±0.3, 0.7±0.4, 0.7±0.1, and 1.1±0.5 mm respectively. Correspondingly, the estimated diameter are found to be 11.7±0.6 mm, 11.7±0.3 mm, 10.3±0.3 mm, and 12.1±0.5 mm respectively.

Fig. 7 shows an example of A-mode echo signals as depicted in the first three sub-figures, illustrating variations at different time instances with h = 25 mm above the tube; and the bottom sub-figure is E_M values derived from the A-mode signals collected over a duration using the method depicted in Equation. (5). All the sub-figures are displayed against depth.

Based on the M-mode processing results, the depth of the top and bottom walls of the tube could be estimated. Table II summarizes the estimated depth of the top wall of the tube h_M and tube diameter in different experimental settings. Specifically, the estimated depths of the top tube wall were reported as 11.3±0.6 mm, 15.7±0.3 mm, 19.2±0.6 mm and 26.7±1.2 mm, corresponding to different depth settings of 10, 15, 20, and 25 mm. The tube diameter was estimated by identifying two peaks within the M-mode signal and calculating the difference between them. The results were found to be 7.2±1.1 mm, 7±1.8 mm, 7.3±1.2 mm, and 7.4±0.7 mm.

B. System efficacy assessment results

In all six trials, the robot successfully identified the tube's location and accurately positioned the needle guide. The

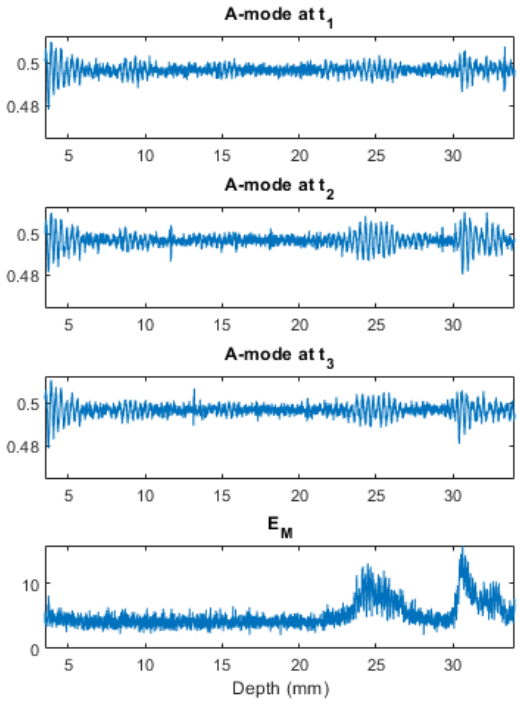

Fig. 7. The first three sub-figures show the examples of A-mode signals recorded at different time stamps (t_1, t_2 and t_3). The bottom sub-figure shows the energy over FFT of the M-mode signal, which is constructed by stacking the A-mode signal along time scale.

TABLE II

THE ESTIMATED DEPTH h_M AND THE TUBE DIAMETER ϕ_M BASED ON THE M-MODE SIGNAL IN DIFFERENT EXPERIMENTAL SETTINGS.

h (mm)	10	15	20	25
h_M (mm)	11.3±0.6	15.7±0.3	19.2±0.6	26.7±1.2
ϕ_M (mm)	7.2±1.1	7±1.8	7.3±1.2	7.4±0.7

success was evidenced by the experimenter's ability to insert the needle and precisely reach the top wall of the tube.

The average execution time of the whole procedure is 88 s. This duration includes 40 s for horizontal scanning, 10 s dedicated to Doppler signal processing, and 3 s for M-mode measurement and processing. The remaining time is allocated variably for repositioning the *Mainbody* and *Needle guide*.

C. Preliminary test results on human volunteers

The subject underwent the testing procedure three times. In all trials, the robot successfully detected periods of Doppler echoes indicative of the CFA location and estimated its depth.

As illustrated in Fig. 8, replicating the precise orientation of the B-mode transducer for CFA measurement to match that of the M-mode transducer used by the robot was found difficult. Therefore, we were able to qualitatively confirm that B-mode imaging, aligned with the stickers, provided visibility of the CFA beneath the surface. However, this

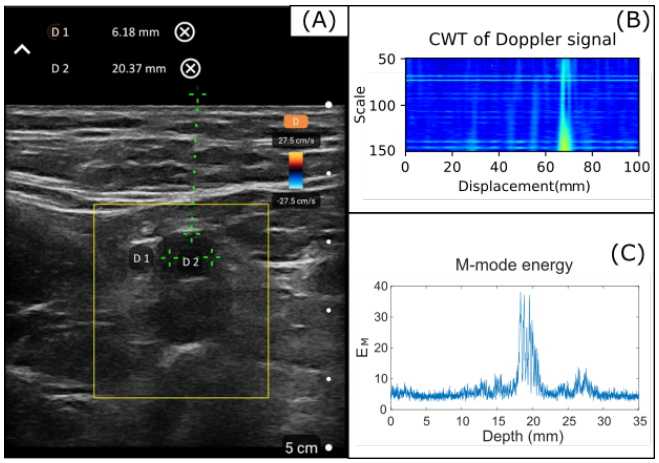

Fig. 8. The experimental result on human subject: (A) the B-mode US image measured on the robot detected site, (B) the CWT of the Doppler signal during a robotic scanning, and (C) the measured M-mode energy against the depth.

approach did not permit a quantitative assessment of the central error. Despite this limitation, by aligning the B-mode device with the CFA's central line, we successfully measured its depth. These measurements were then compared with the depth calculations derived from the M-mode signal, allowing for a qualitative analysis of accuracy.

The robot determined the depth of the CFA's top wall of the subject and its diameter to be 19.3 mm and 7.1 mm respectively. Comparison with B-mode US imaging confirmed these findings, revealing depths of 20.4 mm and diameters of 6.2 mm respectively.

VII. Discussions

The characterization outcomes from the water tank experiments reveal that both the M-mode and Doppler transducers accurately detect the pulsatile tube in both horizontal and vertical orientations with high precision. Considering that the diameter of CFA normally ranges from 6 to 10 mm, the robotic accuracy of less than 2 mm is deem sufficient for this application. Moreover, the tube diameters measured by these transducers match the actual dimensions across various depth settings, demonstrating their reliability, while the measurement error can be due to the probe diffusion.

The efficacy of the whole robotic system is demonstrated through experiments conducted with both a water tank setup and human subjects. In the water tank experiments, we observe that the needle can be accurately inserted into the tube following the detection and the precise positioning of the needle guide by the robot in all trials. In tests involving human subjects, the location and depth of the CFA as determined by the robot are consistent with measurements obtained using a B-mode US device, further affirming the system's accuracy and reliability. In addition, the robot meets the criteria for portability giving the fact of weighing just 1 kg. Moreover, the entire procedure is completed in under 1.5 min, emphasizing its efficiency.

VIII. Conclusion

In this study, we present a portable robot which is able to guide physician in CFA access. A novel sensory solution based on a single Doppler transducer and a single M-mode transducer is proposed and developed. A structured approach, from component assessment to full-system evaluation and preliminary human trials, ensures a comprehensive characterization of the robotic system's capabilities and potential clinical utility. Nevertheless, the authors acknowledge the limitations of this study, notably that only one human subject participated, which is insufficient for drawing definitive conclusions about the system's efficacy. More experiments will be conducted in the future study to further validate our findings. Another limitation is related to the need of an external physician to place the device on the correct femoral triangular region before activating the robot. The current design does not consider the adjusting the probes' position along the leg and its orientation aligning with the vessel direction. Also, additional sensing technologies for guiding needle insertion such as tip tracking [11] and puncture detection [12], [13] can be necessary to be integrated for assuring the success rate.

References

[1] E. M. Campion and C. J. Fox, "Prehospital hemorrhage control and reboa," *Current Trauma Reports*, vol. 5, pp. 129–136, 2019.

[2] A. Ammar, L. Ali, and A. Furqan, "A randomized comparison of ultrasound guided versus blindly placed radial arterial catheters," *Journal of Postgraduate Medical Institute*, vol. 31, no. 1, 2017.

[3] C. A. Troianos, G. S. Hartman, K. E. Glas, N. J. Skubas, R. T. Eberhardt, J. D. Walker, S. T. Reeves *et al.*, "Guidelines for performing ultrasound guided vascular cannulation: recommendations of the american society of echocardiography and the society of cardiovascular anesthesiologists," *Journal of the American Society of Echocardiography*, vol. 24, no. 12, pp. 1291–1318, 2011.

[4] M. Koskinopoulou, Z. Cheng, A. Acemoglu, D. G. Caldwell, and L. S. Mattos, "Robotic devices for assisted and autonomous intravenous access," *IEEE Transactions on Medical Robotics and Bionics*, 2023.

[5] A. I. Chen, M. L. Balter, T. J. Maguire, and M. L. Yarmush, "Deep learning robotic guidance for autonomous vascular access," *Nature Machine Intelligence*, vol. 2, no. 2, pp. 104–115, 2020.

[6] N. Zevallos, E. Harber, K. Patel, Y. Gu, K. Sladick, F. Guyette, L. Weiss, M. R. Pinsky, H. Gomez, J. Galeotti *et al.*, "Toward robotically automated femoral vascular access," in *2021 International Symposium on Medical Robotics (ISMR)*. IEEE, 2021, pp. 1–7.

[7] M. Koskinopoulou, A. Acemoglu, V. Penza, and L. S. Mattos, "Dual robot collaborative system for autonomous venous access based on ultrasound and bioimpedance sensing technology," in *2023 IEEE International Conference on Robotics and Automation (ICRA)*. IEEE, 2023, pp. 4648–4653.

[8] L. J. Brattain, T. T. Pierce, L. A. Gjesteby, M. R. Johnson, N. D. DeLosa, J. S. Werblin, J. F. Gupta, A. Ozturk, X. Wang, Q. Li *et al.*, "Ai-enabled, ultrasound-guided handheld robotic device for femoral vascular access," *Biosensors*, vol. 11, no. 12, p. 522, 2021.

[9] L. W. Spector KS, "Optimizing safe femoral access during cardiac catheterization." 2001.

[10] M. B. Nørløv, "Medical device prototyping and product development management," 2023.

[11] Z. Cheng, S. L. B. Sørensen, M. W. Olsen, R. L. Eriksen, and T. R. Savarimuthu, "Needle tip tracking based on optical imaging and ai," *IEEE Sensors Journal*, vol. 24, no. 17, pp. 28 145–28 153, 2024.

[12] Z. Cheng, B. L. Davies, D. G. Caldwell, and L. S. Mattos, "A hand-held robot for precise and safe pivc," *IEEE Robotics and Automation Letters*, vol. 4, no. 2, pp. 655–661, 2019.

[13] Z. Cheng, M. Koskinopoulou, S. Bano, D. Stoyanov, T. R. Savarimuthu, and L. S. Mattos, "Sensing technologies for guidance during needle-based interventions," *IEEE Transactions on Instrumentation and Measurement*, vol. 73, pp. 1–15, 2024.